Measurement of deep states in hole doped organic semiconductors

Debdutta Ray and K. L. Narasimhan

Citation: Journal of Applied Physics **103**, 093711 (2008); doi: 10.1063/1.2919058
View online: http://dx.doi.org/10.1063/1.2919058
View Table of Contents: http://scitation.aip.org/content/aip/journal/jap/103/9?ver=pdfcov
Published by the AIP Publishing

Measurement of deep states in hole doped organic semiconductors

Debdutta Ray and K. L. Narasimhan[a)]
Department of Condensed Matter Physics and Material Sciences, Tata Institute of Fundamental Research, Colaba, Mumbai 400005, India

(Received 14 December 2007; accepted 6 March 2008; published online 8 May 2008)

In this paper, we report on the electrical properties of hole doped N,N'-diphenyl-N,N'-bis(3-methylphenyl)-(1,1′-biphenyl)-4,4′-diamine and tris(8-hydroxyquinoline) aluminum. Tetrafluorotetracyanoquinodimethane is used as the dopant. From the frequency dependence of the capacitance measurements, we show that deep levels dominate the capacitance. From the frequency and bias dependence, we estimate the density of deep levels above the Fermi level to be about 10^{17} cm^{-3}. These states presumably arise due to polarization and Coulomb energy fluctuations.
 [DOI: 10.1063/1.2919058]

I. INTRODUCTION

Organic semiconductors find a wide range of applications spanning from light emitting diodes to solar cells.[1–5] To maximize device performance, it is crucial to be able to dope these materials. For instance, doping reduces contact resistance and, thereby, enhances device efficiency.[6–8] One way of doping that has recently emerged is the use of an organic dopant wherein the lowest unoccupied molecular orbital (LUMO) [highest occupied molecular orbital (HOMO)] of the dopant is energetically in the vicinity of the HOMO (LUMO) of the organic semiconductor, thereby facilitating charge transfer.[6,9,10] In this paper, we report on the electrical properties of hole-doped N,N'-diphenyl-N,N'-bis(3-methylpheny1)-(1,1′-biphenyl)-4,4′-diamine (TPD). TPD has been widely used as the hole transporting layer in organic light emitting diodes.[11] In this work, tetrafluorotetracyanoquinodimethane (F_4-TCNQ) is used as the dopant. The LUMO of F_4-TCNQ is energetically in the vicinity of the HOMO of TPD.[10,12] Thus, F_4-TCNQ could act as an acceptor, leading to the formation of TPD^+ and F_4-$TCNQ^-$. The hole is free to move from one TPD molecule to another by hopping. The electrons are likely to be localized on the F_4-TCNQ molecules. This is because at these low doping densities (~3% in this study), the F_4-TCNQ concentration is below the percolation limit for the electrons. This, in effect, leads to (relatively) immobile negative ionized acceptors (F_4-$TCNQ^-$). In this paper, we report on capacitance and electrical transport measurements on doped samples of TPD. From the dc transport measurements, we show that F_4-TCNQ is a deep acceptor in TPD.

II. EXPERIMENT

Thin films of doped TPD were prepared by coevaporating TPD and F_4-TCNQ on patterned indium tin oxide (ITO) substrates for electrical measurements. The individual deposition rates of TPD and F_4-TCNQ were monitored by using three quartz crystal oscillators. The evaporation rates were kept constant for uniform doping through the thickness of the sample. The base pressure of the system was 5×10^{-7} Torr. Both planar and sandwich structures were used. ITO was the Ohmic contact for the F_4-TCNQ doped TPD samples. For measurements in the planar configuration, we used interdigitated ITO electrodes with 100 μm separation. The sandwich device had a configuration of ITO/TPD+F_4-TCNQ (3%) (2000 Å)/semitransparent-Al/LiF. The top LiF was an encapsulation layer. The active area of the device was typically 10^{-2} cm^2. Device transfer from the deposition chamber to the measurement jig was done via a load-lock assembly in a nitrogen environment. All measurements were carried out in vacuum. For photocurrent measurements, the incident light on the sample was chopped at 11 Hz by using a mechanical chopper.[13] The photocurrent was measured using a lock-in amplifier. Some electrical measurements were also performed *in situ* in the deposition chamber immediately after growth. We first discuss transport in planar configuration and present evidence for doping of TPD. We then discuss the capacitance measurements in the sandwich samples followed by dark and phototransport in the sandwich structures.

III. RESULTS AND DISCUSSION

A. Dark conductivity in planar samples

Figure 1 is a plot of the conductivity as a function of $1000/T$ for a planar doped sample. The conductivity at room temperature is 6×10^{-8} $(\Omega\ cm)^{-1}$. This is comparable to the data reported earlier for F_4-TCNQ doped TPD samples.[14] The conductivity of the doped samples is at least three orders of magnitude larger than that for the undoped TPD sample. We hence conclude that F_4-TCNQ is an electrically active dopant in TPD. The temperature dependence of the dc electrical conductivity can be written as

$$\sigma = \sigma_0 \exp(-E_A/kT). \quad (1)$$

We find $\sigma_0=0.15$ $(\Omega\ cm)^{-1}$ and $E_A=0.38$ eV. If we write $E_A=E_F-E_V$, where E_F is the Fermi level and E_V is the HOMO level of TPD, then E_F is at the most 0.38 eV above the HOMO level of TPD. The position of E_F is determined by charge neutrality and should be located close to the LUMO level of F_4-TCNQ for the doping concentrations used in our experiments. Photoemission experiments suggest that

a)Author to whom correspondence should be addressed. Electronic mail: kln@tifr.res.in.

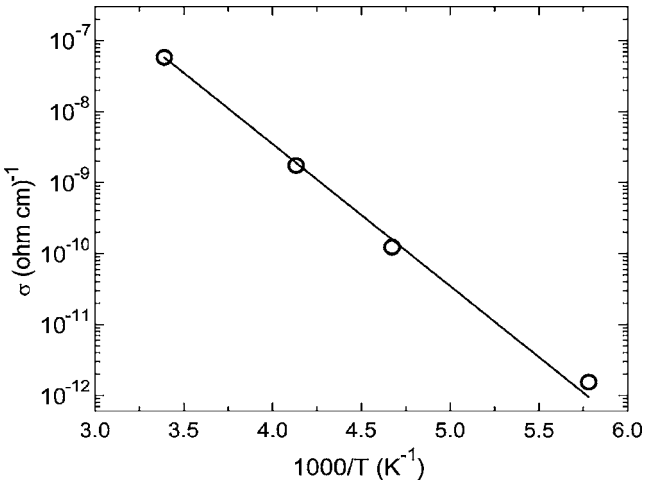

FIG. 1. A plot of conductivity as a function of $1000/T$ for a planar doped TPD sample. The activation energy of the conductivity is 0.38 eV.

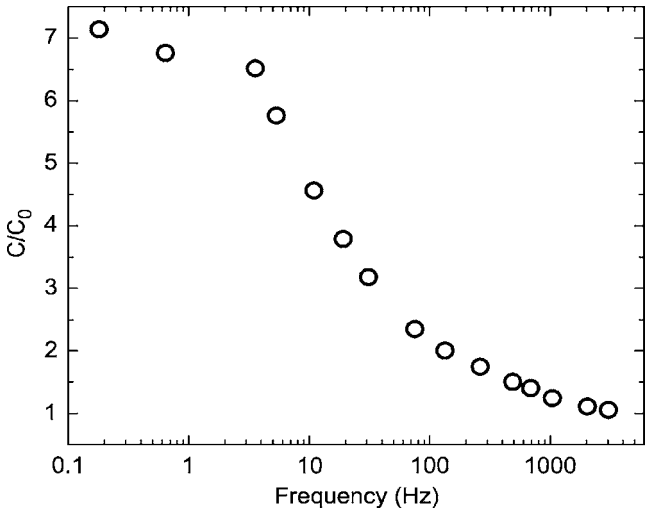

FIG. 2. A plot of the frequency dependence of the normalized capacitance C/C_0 (C_0 being the geometric capacitance) for a doped TPD sample. For frequency less than 5 Hz, the capacitance was recorded by measuring the displacement current. The value of C_0 is 14 $\mathrm{nF/cm^2}$.

the HOMO of TPD and the LUMO of F_4-TCNQ are at −5.44 and −5.24 eV, respectively, with respect to the vacuum level.[10,12] We hence expect E_F to be located 0.2 eV above the HOMO level of TPD. Since the energy resolution in the photoemission measurements is 0.15 eV, the measured electrical activation energy of 0.38 eV is not inconsistent with the photoemission data.[10,15] Alternatively, if the mobility is also thermally activated, the activation energy (E_A) of conductivity can be expressed as[16,17]

$$E_A = (E_F - E_V) + E_M, \tag{2}$$

where E_M is the thermal activation energy of the hole mobility $[\mu = \mu_0 \exp(-E_M/kT)]$. If $(E_F - E_V) = 0.2$ eV, as suggested by photoemission experiments, then the hole mobility is thermally activated with an activation energy of 0.18 eV—hole transport takes place by a thermally activated hopping process.

Charge transport in organic semiconductors is not very well understood. Some models invoke hopping transport in a Gaussian band tail and others assume hopping in an exponential band tail.[18,19] The mobility strongly depends on temperature and carrier concentration. The experiments reported here cannot resolve these questions, which are beyond the scope of this work.

B. Capacitance measurements

Capacitance measurements can provide information of gap states in doped systems. Figure 2 shows the zero bias normalized capacitance (normalized to the geometrical capacitance C_0) for a 2000 Å thick doped TPD sample sandwiched between ITO and Al electrodes. We see from Fig. 2 that the value of the capacitance depends on frequency and is about seven times the geometric capacitance at a low frequency (less than 5 Hz). This is direct evidence for the presence of space charge layers and confirms that the Fermi level in F_4-TCNQ doped TPD has moved toward the HOMO level of TPD. We now try to understand the zero bias frequency dependence of capacitance.

When a semiconductor is sandwiched between two asymmetric electrodes, there is a built-in electric field that arises due to the difference in the Fermi levels between the two electrodes. If the carrier density in the semiconductor is small, then a uniform field develops across the semiconductor as there are no free charges to screen out the field in the body of the semiconductor. The capacitance is independent of the modulating frequency and is given by the geometric capacitance. This is the case for the undoped TPD samples. If the semiconductor is doped, the built-in field is screened by the dopant charge. This gives rise to band bending and a space charge region. If the dopants are shallow donors (acceptors), the depletion region is well defined. The capacitance in this case arises from modulation of charge at the edge of the depletion region. The capacitance is independent of frequency (limited only by the dielectric relaxation time) and is given by $C = \varepsilon\varepsilon_0 A/D$, where ε is the dielectric constant, A is the area, and d is the width of the depletion region.

The situation is very different if the dopant levels are deep or if the deep level concentration is greater than the shallow dopant concentration.[20–23] Doped a-Si:H is a good example of a system wherein deep levels dominate the low frequency capacitance behavior.[20] The expected frequency dependence at zero dc bias for such a system is described as follows. Figure 3(a) is a schematic of the band bending of a doped sample with a continuous distribution of gap states. Upon applying a small ac bias, the surface potential is modulated by $\pm d\psi_s$. At zero (and small reverse) bias, the quasi-Fermi level (E_{fp}) is constant throughout the sample.[20,21] As the surface potential is modulated at an angular frequency ω, the energy levels follow the potential and some of them cross E_F. To contribute to the total modulated charge (and, hence, capacitance), majority carrier emission from the deep level (trap) needs to take place. The response time for majority carrier emission from the trap is given by

$$\tau = \tau_0 \exp(\Delta E/kT). \tag{3}$$

All states that are characterized by $\omega\tau \leq 1$ can change their charge state and will contribute to the capacitance. This is schematically shown in Fig. 3(a), wherein A represents the

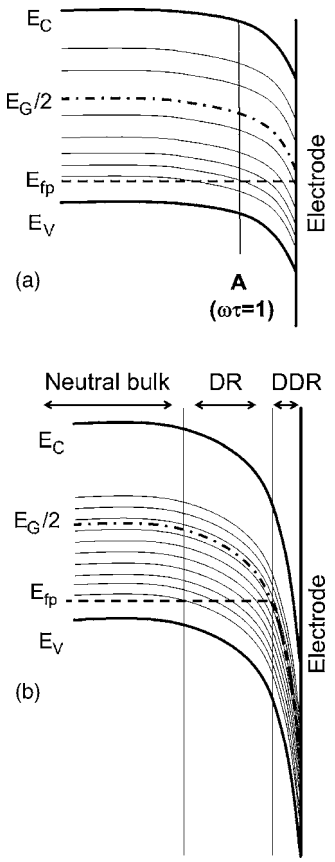

FIG. 3. The energy level alignment of a doped TPD device near the Al electrode is shown (a) when the device is at small reverse bias and (b) when it is at large reverse bias. DR and DDR are acronyms for the depletion region and deep depletion region, respectively.

location in the depletion region where $\omega\tau=1$. All traps to the left of A can follow the ac voltage and will contribute to the capacitance (C_{sc}). The region to the right of A behaves like an insulator (C_{ins}). The total capacitance consists of two capacitors in series, C_{ins} and C_{sc}.[20,22] As ω decreases, point A moves closer to the contact as states deeper in energy can follow the applied frequency and contribute to the capacitance. The frequency dependence arises due to the presence of deep levels below E_F. This explains the frequency dependence of the capacitance seen in Fig. 2. Below 5 Hz, the capacitance is dominated by C_{sc} as C_{ins} has become very large. To get an approximate estimate of the density of states above E_F, we assume a constant density of states above E_F of value g_0. In this case, $C_{sc}=A\sqrt{(qg_0\varepsilon\varepsilon_0)}$.[20,23] From the value of the capacitance at the lowest frequency in Fig. 2, we estimate g_0 to be 2×10^{17} cm^{-3} eV^{-1}.

Similar results are also observed for tris(8-hydroxyquinoline) aluminum (AlQ_3) films doped with F_4-TCNQ. Figure 4 shows the frequency dependence of the capacitance for AlQ_3 film doped with 4% of F_4-TCNQ. Since the HOMO level of AlQ_3 is deeper than that in TPD, there is a smaller dispersion of the capacitance and it reaches the geometrical capacitance at a lower frequency than in TPD. The density of states (g_0) above E_F is estimated to be around 10^{16} cm^{-3} eV^{-1}. This is around 20 times smaller than that measured in TPD. This is because the HOMO level in

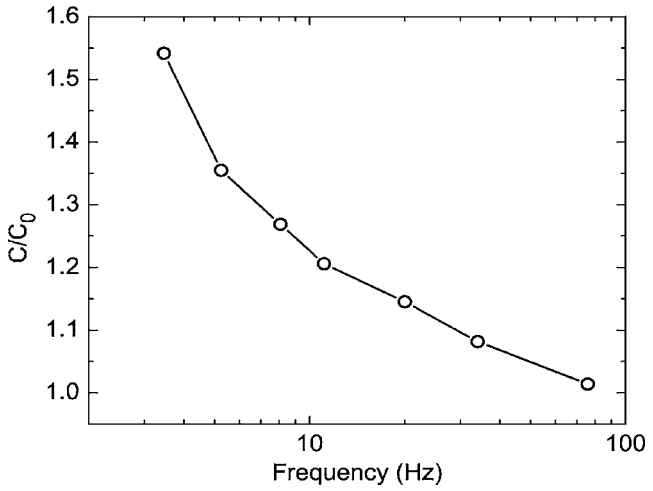

FIG. 4. A plot of the frequency dependence of the capacitance (C_0 is the geometric capacitance) for a F_4-TCNQ doped AlQ_3 sample.

AlQ_3 is deeper than that in TPD by around 0.4 eV. The capacitance measurements in AlQ_3 hence measure the states in the vicinity of E_F.

We now study the voltage dependence of low frequency capacitance in reverse bias. Figure 5 shows the capacitance as a function of the reverse bias for a doped TPD sample. The data is corrected for series resistances that arise from the sample and from the external circuit.[23] The capacitance decreases as we increase the reverse bias. In a semiconductor wherein the capacitance is determined by the shallow acceptor density, this result is easy to understand and is related to the increase in the depletion layer with increase in reverse bias voltage. For the case wherein deep levels dominate the capacitance, the decrease in capacitance with increasing reverse bias can be understood as follows:[20] At a small reverse bias, E_{fp} is constant through the semiconductor. With increasing reverse bias, point A [Fig. 3(a)] moves away from the surface and farther into the semiconductor bulk. The total capacitance is due to two capacitors (C_{sc} and C_{ins}) in series. C_{sc} is bias independent. With increasing reverse bias, C_{ins}

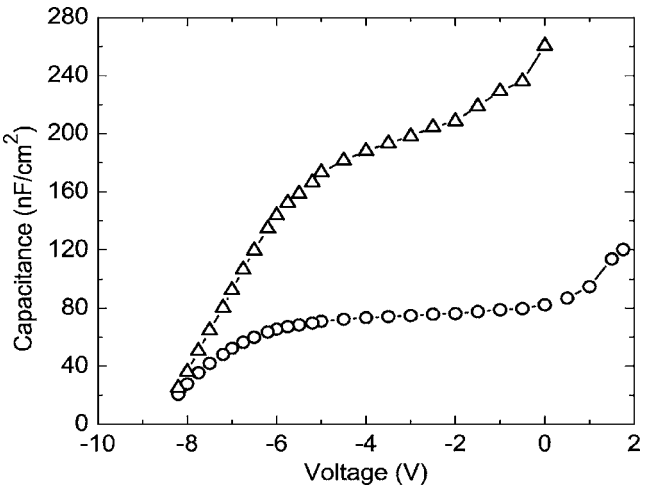

FIG. 5. A plot of the voltage dependence of the capacitance for a 2000 Å thick TPD device. The plot shows the measured capacitance (-○-) and C_{ins} (-Δ-). C_{ins} was calculated by assuming that the capacitance at slight forward bias is the measure of C_{sc}.

decreases and eventually dominates the capacitance. This explains the decrease of the capacitance with increasing reverse bias. This "insulator" region is termed in the *a*-Si:H literature as the depletion region. The width of the depletion region is determined by the density of deep states. At a large reverse bias, E_{fp} is no longer constant and follows the band bending.[20] This is schematically shown in Fig. 3(b). This happens at a voltage when the intrinsic level $E_G/2$ crosses the Fermi level. E_{fp} follows $E_G/2$ in the region next to the contact. This region is known as the deep depletion region. Since E_{fp} follows the band bending, there will be no charge modulation in this region. Thus, this region also behaves like an insulator. At a large voltage, almost all of the potential drop is across the deep depletion region and for a given bias, the integrated density of states between E_F and $E_G/2$ is given by the profiler formula[20,24]

$$N_{C\text{-}V} = -\frac{C^3}{\varepsilon q A^2}\left[\frac{dC}{dV}\right]^{-1}, \tag{4}$$

where the *C-V* is measured at a low frequency. We note that E_F denotes the position of the Fermi level in the neutral bulk of the semiconductor. The measured capacitance is due to the series capacitance of C_{ins} and C_{sc}. The profiler formula given in Eq. (4) is clearly valid only when $C_{ins} < C_{sc}$. To estimate C_{ins} at different voltages, we use the low frequency capacitance at a small forward bias as a measure of C_{sc}. Figure 5 also shows C_{ins}, which is calculated by subtracting out the contribution of C_{sc} from the total measured capacitance. We see from Fig. 5 that C_{sc} dominates the measured capacitance to about 6 V reverse bias. The application of the profiler formula is valid only for a reverse bias greater than 6 V. Using Eq. (4), we estimate the density of states between E_F and $E_G/2$ to be 10^{17} cm^{-3}. This is in good agreement with the number obtained from the zero bias low frequency capacitance measurements.

We mention in passing that the frequency dependence of capacitance has been reported in undoped organic semiconductors.[25–27] However, these experiments were carried out in forward bias. The capacitance arises due to injection of charge carriers from the contacts and a distribution of transit times in the sample. The change in the capacitance is also relatively small (~5%). The results reported here are in reverse bias and due to the space charge arising from a change in the charge state of the deep levels. Depending on the position of the Fermi level, the change can be large (~700%) for the doped TPD samples reported here. The physical phenomenon is very different in the two experiments.

In conclusion, we find that the capacitance of hole doped TPD and AlQ_3 samples exhibit strong frequency dependence in reverse bias. This is evidence for the presence of deep states at energies above E_F. These states arise, most probably, due to the broadening of the HOMO levels. Possible reasons for broadening of the HOMO level could be polarization energy corrections and Coulomb energy fluctuations. Capacitance measurements provide an estimate of the integrated density of states above the Fermi level and can be used as a measure of the disorder.

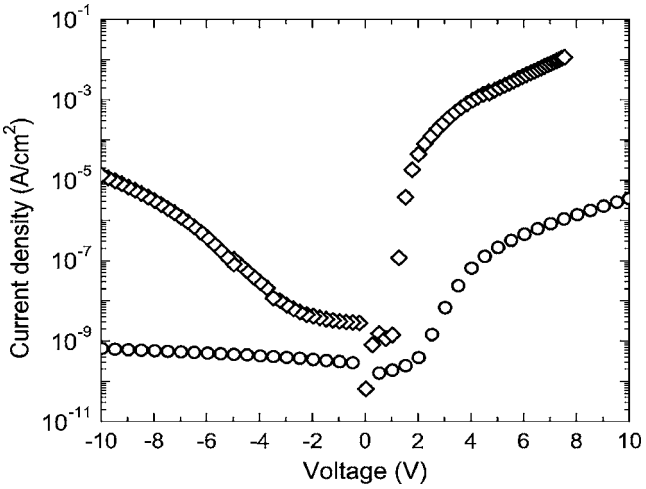

FIG. 6. A plot of the dark current density as a function of voltage for 2000 Å thick samples of (a) undoped TPD (○) and (b) doped TPD (◇).

C. Current-voltage measurements

Figure 6 shows the dark current characteristics of 2000 Å thick undoped TPD and F_4-TCNQ doped TPD sandwich devices. In forward bias, the ITO electrode is the anode. The dark current in forward bias turns on at a lower voltage for the doped sample than for the undoped sample. The presence of the doped layer lowers the barrier for hole injection into TPD by efficient carrier tunneling into the semiconductor.[28] The reverse leakage current also increases in the doped sample. One possibility for the larger reverse bias leakage is efficient electron injection from ITO into the F_4-TCNQ LUMO levels with electron transport taking place by carrier hopping along these levels. To verify whether the reverse current is dominated by electron hopping along the F_4-TCNQ molecules, we measured the dark current in a system wherein the F_4-TCNQ is dispersed in polycarbonate that is an insulator. The F_4-TCNQ concentration is similar to that used in the doped TPD films. The device structure is ITO/polycarbonate+F_4-TCNQ/Al. Figure 7(a) shows the current-voltage curve for both the neat polycarbonate films and the films doped with F_4-TCNQ. The doped polycarbonate sample has a higher conductivity than the doped sample. The current-voltage characteristic is symmetric. The low frequency capacitance of this device is equal to the geometric capacitance, which confirms that no electronic doping has taken place. Figure 7(b) is a comparison of the current as a function of electric field for F_4-TCNQ doped TPD, AlQ_3, and polycarbonate sandwich devices with a similar F_4-TCNQ concentration. The dark current for the AlQ_3 doped films is similar to that for the doped polycarbonate samples. The current in the doped TPD films is comparable to the current in the doped polycarbonate films at a large reverse bias. All of these results suggest that the reverse current in the doped TPD films is dominated by electron hopping along F_4-TCNQ molecules. At low fields, the current density in the doped TPD films is smaller than that observed in the doped polycarbonate films. The lower levels of current in the doped TPD films could be due to the following reasons. In a doped TPD film, Coulomb disorder may broaden the LUMO states of F_4-TCNQ. In such a case, the conduc-

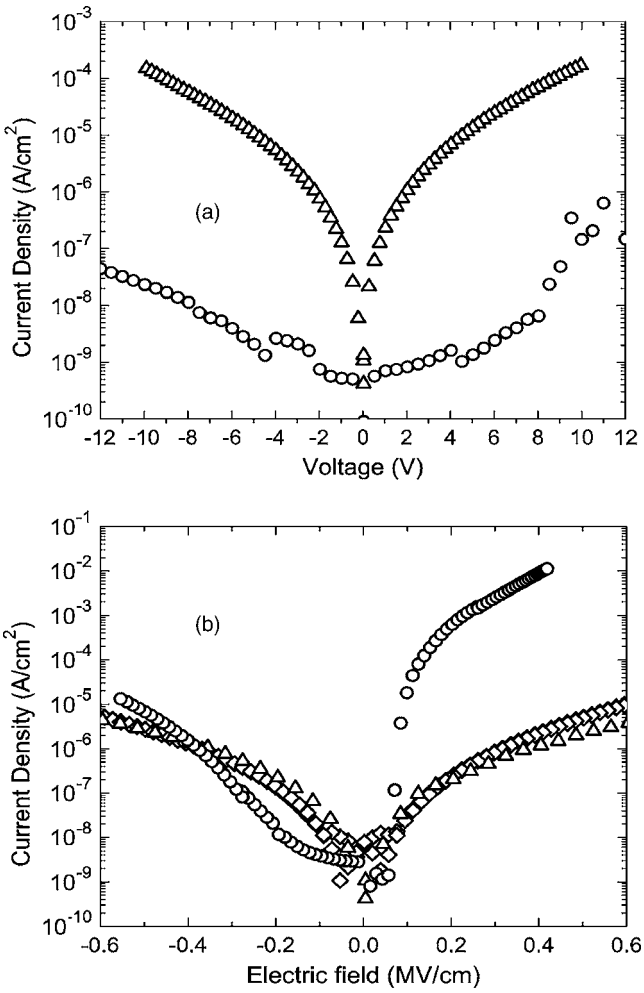

FIG. 7. The dark current voltage plot of a neat polycarbonate film (○) and one where F_4-TCNQ is added to it (Δ) are shown in graph (a). Graph (b) compares the dark current for F_4-TCNQ doped TPD (○), AlQ_3 (◇), and polycarbonate (Δ) films.

tance will be different from that observed in the undoped cases. Another possible reason is that due to the presence of the space charge region, the electric field is not constant through the sample and could be much smaller in the neutral region.

We now discuss the photoconductivity in the doped TPD samples. The photocurrent in neat TPD is due to bulk carrier generation in reverse bias.[13] The photocurrent, for such a case, can be expressed as[13,29]

$$J_{PC} = qG\eta\mu\tau F, \tag{5}$$

where G is the volume density of photons absorbed in the active region (depletion region) of the device, q is the electronic charge, F is the electric field, η is the carrier generation efficiency, and τ is the carrier trapping time. Figure 8 shows the photocurrent as a function of voltage for a 2000 Å thick (ITO/TPD+F_4-TCNQ(3%) (2000 Å)/semitransparent-Al/LiF) sample illuminated at 360 nm through the semitransparent Al electrode. The photocurrent increases with (reverse) bias and goes through a maximum at −7.5 V. In reverse bias, the Al electrode is the anode. The holes move away from the anode and get collected at the far ITO end. In the doped TPD samples, the applied voltage primarily drops

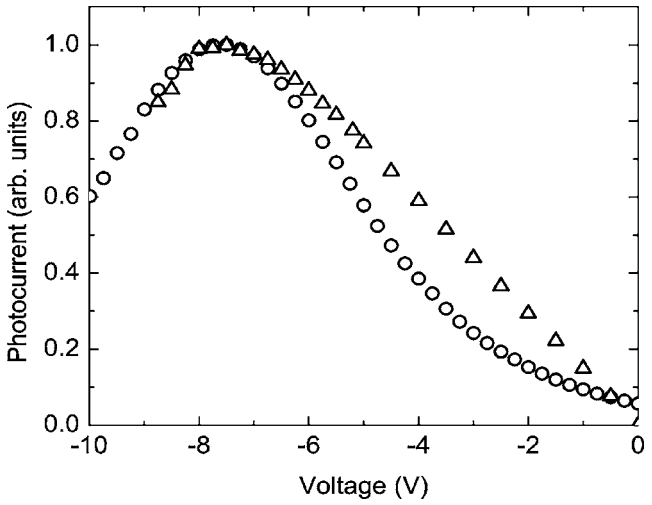

FIG. 8. A plot of the measured (○) and calculated [Δ, by using Eq. (5)] photocurrents as a function of applied reverse bias.

across the depletion region in reverse bias. We approximate the electric field (F) in the junction to be V/W_{dep}, where V is the applied bias and W_{dep} is the depletion width. The depletion width can be obtained from capacitance measurements for voltages wherein the contribution to total capacitance from C_{sc} is negligible, i.e., when C_{ins} dominates the capacitance. This is a good approximation for a voltage greater than 6 V reverse bias in our sample. The photocurrent calculated by using Eq. (5) is also plotted in Fig. 8. Although the number of photons absorbed increases with the depletion width, the electric field falls off faster leading, to a decrease in the photocurrent at a higher voltage. This qualitatively explains the bias dependence of the photoresponse of the sample. The $\eta\mu\tau$ product is calculated to be 3×10^{-13} cm^2/V. This is an order of magnitude larger than that for TPD. A simple explanation for this increase is that the lifetime (τ) has increased because of doping. This can happen if the recombination centers are filled up with holes thereby enhancing the lifetime.

The recombination kinetics can be probed by measuring the photoconductivity in planar structures. If the recombination is Langevin type, the photocurrent will increase as square root of intensity.[30] Figure 9 shows the photocurrent in a planar sample as a function of excitation intensity. From the plot, the photocurrent is observed to depend on the excitation intensity (I) as

$$J_{PC} \propto I^{0.9}. \tag{6}$$

This shows that the recombination is not bimolecular. The carrier lifetime is controlled by traps that act as recombination centers in the vicinity of the Fermi level. For the light intensity used in these measurements, the quasi-Fermi level under illumination is not very different from the dark Fermi level as the photoconduction in these materials is small.

IV. CONCLUSION

In conclusion, we have studied electrical transport of F_4-TCNQ doped TPD. From dc planar measurements and capacitance measurements, we provide evidence for hole

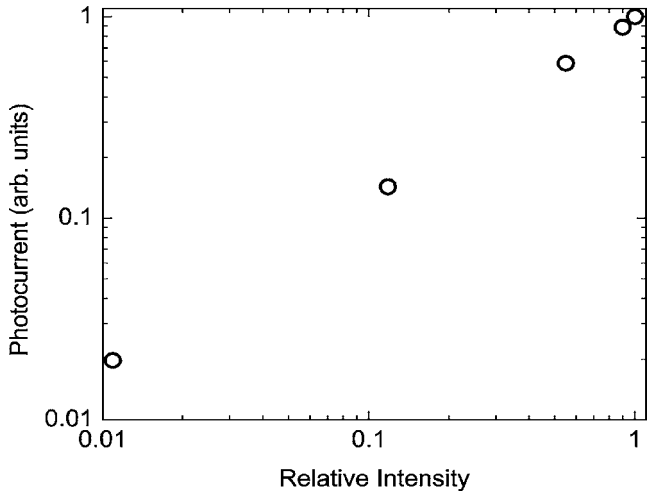

FIG. 9. A plot of the intensity dependence of the photocurrent for a planar TPD device.

doping of TPD by F_4-TCNQ. The capacitance of doped samples is strongly frequency dependent as the capacitance is determined by the density of deep states. The density of states between E_F and $E_G/2$ is about 10^{17} cm^{-3} for TPD. These states arise due to the broadening of the HOMO level due to polarization corrections and Coulomb energy fluctuations. Intensity dependence of photocurrent measurements in planar samples suggest that the carrier lifetime is governed by traps and not by Langevin recombination.

ACKNOWLEDGMENTS

We thank Mr. Meghan Patankar for his help.

[1]C. W. Tang and S. A. VanSlyke, Appl. Phys. Lett. **51**, 913 (1987).
[2]P. Peumans, A. Yakimov, and S. R. Forrest, J. Appl. Phys. **93**, 3693 (2003).
[3]J. Xue, S. Uchida, B. P. Rand, and S. R. Forrest, Appl. Phys. Lett. **85**, 5757 (2004).
[4]C. J. Brabec, N. S. Sariciftci, and J. C. Hummelen, Adv. Funct. Mater. **11**, 15 (2001).
[5]J. J. M. Halls, C. A. Walsh, N. C. Greenham, E. A. Marseglia, R. H. Friend, S. C. Moratti, and A. B. Holmes, Nature (London) **376**, 498 (1995).
[6]J. Blochwitz, M. Pfeiffer, T. Fritz, and K. Leo, Appl. Phys. Lett. **73**, 729 (1998).
[7]X. Zhou, M. Pfeiffer, J. Blochwitz, A. Werner, A. Nollau, T. Fritz, and K. Leo, Appl. Phys. Lett. **78**, 410 (2001).
[8]W. Gao and A. Kahn, Org. Electron. **3**, 53 (2002).
[9]B. Maennig, M. Pfeiffer, A. Nollau, X. Zhou, K. Leo, and P. Simon, Phys. Rev. B **64**, 195208 (2001).
[10]W. Gao and A. Kahn, Appl. Phys. Lett. **79**, 4040 (2001).
[11]G. Gu, P. E. Burrows, S. Venkatesh, S. R. Forrest, and M. E. Thompson, Opt. Lett. **22**, 172 (1997).
[12]R. Schlaf, B. A. Parkinson, P. A. Lee, K. W. Nebesny, and N. R. Armstrong, Appl. Phys. Lett. **73**, 1026 (1998).
[13]D. Ray, M. P. Patankar, G. H. Dohler, and K. L. Narasimhan, J. Appl. Phys. **100**, 113727 (2006).
[14]M. Pfeiffer, K. Leo, X. Zhou, J. S. Huang, M. Hofmann, A. Werner, and J. Blochwitz-Nimoth, Org. Electron. **4**, 89 (2003).
[15]W. Gao and A. Kahn, J. Appl. Phys. **94**, 359 (2003).
[16]W. Brutting, S. Berleb, and A. G. Muckl, Org. Electron. **2**, 1 (2001).
[17]S. Heun and P. M. Borsenberger, Chem. Phys. **200**, 245 (1995).
[18]R. Coehoorn, W. F. Pasveer, P. A. Bobbert, and M. A. J. Michels, Phys. Rev. B **72**, 155206 (2005).
[19]W. F. Pasveer, J. Cottaar, C. Tanase, R. Coehoorn, P. A. Bobbert, P. W. M. Blom, D. M. de Leeuw, and M. A. J. Michels, Phys. Rev. Lett. **94**, 206601 (2005).
[20]J. D. Cohen and D. V. Lang, Phys. Rev. B **25**, 5321 (1982).
[21]G. I. Roberts and C. R. Crowell, J. Appl. Phys. **41**, 1767 (1970).
[22]C. R. Crowell and K. Nakano, Solid-State Electron. **15**, 605 (1972).
[23]D. K. Sharma, K. L. Narasimhan, S. Kumar, B. M. Arora, W. Paul, and W. A. Turner, J. Appl. Phys. **65**, 1996 (1989).
[24]S. M. Sze, *Physics of Semiconductor Devices*, 2nd ed. (Wiley-Interscience, New York, 1981), pp. 245–249.
[25]H. C. F. Martens, H. B. Brom, and P. W. M. Blom, Phys. Rev. B **60**, R8489 (1999).
[26]F. So, B. Krummacher, M. K. Mathai, D. Poplavskyy, S. A. Choulis, and V. Choong, J. Appl. Phys. **102**, 091101 (2007).
[27]S. W. Tsang, S. K. So, and J. B. Xu, J. Appl. Phys. **99**, 013706 (2006).
[28]J. Drechsel, M. Pfeiffer, X. Zhou, A. Nollau, and K. Leo, Synth. Met. **127**, 201 (2002).
[29]R. S. Crandall, in *Hydrogenated Amorphous Silicon, Semiconductors and Semimetals, Part B: Optical Properties*, Vol. 21, edited by Jacques I. Pankove (Academic Press, Inc., Orlando, 1984), pp. 245–297.
[30]M. Gailberger and H. Bassler, Phys. Rev. B **44**, 8643 (1991).